AIAA JOURNAL
Vol. 50, No. 12, December 2012

Large-Eddy Simulation of Shock/Boundary-Layer Interaction

Abdellah Hadjadj*
Institut National des Sciences Appliquées de Rouen, 76801 Saint Etienne du Rouvray, France

DOI: 10.2514/1.J051786

This work considers numerical simulations of supersonic flows when shock/turbulent boundary-layer interaction occurs. Such flows reveal the existence of complex mechanisms, which need to be carefully investigated for efficient design of propulsion systems. In this study, large-eddy simulation is used to investigate unsteady mechanisms. Because a shock-capturing scheme is used, a hybrid numerical scheme has been developed to reduce its dissipative properties. The issue of the generation of coherent turbulent inlet boundary conditions is also addressed. To avoid introducing artificial low-frequency modes that could affect the interaction, a method based on a digital-filter approach is used to provide a synthetic-inflow condition over a relatively short distance. The obtained results are analyzed and discussed in terms of mean and turbulent quantities. Excellent agreement between large-eddy simulations and experimental data are obtained for both the undisturbed boundary layer and the shock impingement region. In the latter case, oscillations of the reflected shock occurring at low frequencies are observed, in agreement with previous numerical and experimental findings. Moreover, simulations reveal the presence of such frequencies mainly near the shock foot and within the recirculation bubble. This point gives credit to the hypothesis that the instabilities of the reflected shock are due to the intrinsic low-frequency movement of the shock/bubble acting dynamically as a coupled system.

I. Introduction

SHOCK-WAVE/boundary-layer interaction (SWBLI) is a basic fluid-dynamics phenomenon that has both fundamental and practical importance. In space propulsion systems, for instance, accurate estimates of side loads in rocket nozzles require, in part, a detailed study of boundary-layer separation dynamics and the associated shock unsteadiness. Although these phenomena appear to not only depend on the nozzle geometry [1,2], because they have been also revealed in many other configurations such as ducts [3–5], impinging oblique shocks [6], or compression ramps [7,8], their relevance in SWBLI applications and, in particular, the fluctuating pressure loads generated by translating shock waves, pulsating separated flows, and expansions/contractions of the global flowfield which may cause severe structural damages, cannot be ignored by designers of rocket nozzles. In this problem, several viscous phenomena are observed, including a boundary layer with adverse pressure gradients, induced separation, shear layers, and a recirculation bubble; some of the salient features of these phenomena are given in [9–12].

Previous studies have shown that the shock motion has a frequency much lower than the characteristic frequency of the turbulent boundary layer, and that the timescale associated with the low frequency is $\mathcal{O}(10\delta/U_\infty - 100\delta/U_\infty)$, in contrast to the characteristic timescale of the incoming boundary layer, which is $\mathcal{O}(\delta/U_\infty)$. This topic related to the interaction between shock waves and turbulent flows is reviewed in detail by Andreopoulos et al. [13,14]. Basically, the fluctuations may arise from two sources: the interaction between the shock wave and the incoming turbulence or the instabilities in the shock foot related to the downstream flow organization. From experiments made in a Mach 3 compression ramp, Andreopoulos and Muck [13], among others, suggested that the oscillations of the separation shock correlate with the burst frequency of the incoming boundary layer. Unalmis and Dolling [15], Beresh et al. [16], and Hou et al. [17] found correlations between velocity fluctuations in the lower portion of the upstream boundary layer and the shock foot region. The experimental investigation of Ganapathisubramani et al. [8], based on conditional analysis, showed also a link between the large vortical structures formed in the upstream boundary layer and the unsteadiness of the interaction in the case of a compression ramp at Mach 2. The authors noticed that such vortical structures can be as long as 30δ and they are associated with velocity perturbations typically of $\pm 2u_\tau$ (Ganapathisubramani et al. [8] and Adrian et al. [18]), where u_τ is the friction velocity. More recently, Humble et al. [19] identified streamwise-elongated regions of relatively low- and high-speed fluid, and highlighted a statistical link between these structures and the motions of the interaction region.

In contrast, the experiments of an impinging oblique shock flow performed by Dupont et al. [6], as well as the direct numerical simulation (DNS) of Wu and Martin [20] of a compression ramp at Mach 2.9, suggest that the low frequencies of the shock motion are strongly linked to the downstream flow and particularly to the separated bubble. Also, Dolling and Smith [21], Gramman and Dolling [22], and Hou et al. [23] examined the case of interaction produced by a blunt body. They showed that the motion of a shock wave produced by a blunt body scales with the diameter of the blunt body, that is, with the downstream conditions. Moreover, the phase relationships between the shock movement and the recirculation bubble were deduced experimentally and numerically (Dupont et al. [6], Erengil and Dolling [7], Debiève and Dupont [24], and Thomas et al. [25]) on compression ramps and shock impinging. The main finding is the opposition in phase between the pressure signals near the foot of the shock and those in the recirculation bubble. A model was developed by Dupont et al. [6]) based on their experimental data to correlate the low-frequency unsteadiness of the separation shock with the own dynamics of the separation bubble in terms of contractions/expansion. The model considers that the vortex structures convected downstream carry a mass of fluid that must be intermittently reinjected in the separated zone to keep a constant average mass. These vortices are generated by the mixing layer, which is formed from the separation point.

On the other hand, the DNS of Pirozzoli and Grasso [26] showed that the interaction of the coherent structures with the incident shock produces acoustic waves that propagate upstream, thus inducing an oscillatory motion of the separation bubble and a subsequent flapping motion of the reflected shock. It has been also shown

Received 20 December 2011; revision received 28 March 2012; accepted for publication 29 March 2012.

*Professor, National Institute of Applied Sciences, Centre National de la Recherche Scientifique, Unité Mixte de Recherche 6614, Avenue de l'Université, Rouen, France. Member AIAA.

that low-frequency tones occurring in the interaction zone are associated with peaks in the pressure spectra at discrete frequencies and are likely due to a resonance mechanism that establishes in the interaction region, and which has close similarities with those responsible for the generation of tones in cavity flows and screeching jets.

A very limited number of large-eddy simulations (LES) of transonic/supersonic SWBLI have been reported so far. Garnier and Sagaut [27] has carried out a large-eddy simulation of an oblique shock wave impinging upon a turbulent boundary layer at conditions that mimic the experimental conditions of Dupont et al. [28]. They found generally good agreement between the computed mean global quantities, such as skin friction and displacement thickness, and experimental results. However, they were unable to investigate the low-frequency effects, due to reported difficulties to obtain a sufficiently longtime record of the flowfield. In the context, recently Garnier [29] reported results of an advanced computational fluid dynamics (CFD) investigation using a stimulated detached-eddy simulation methodology on the unsteadiness aspects of the three-dimensional SWBLI. When accounting for the whole wind-tunnel span, the simulation showed that corner separations induced by the presence of lateral walls reduce the effective section of the wind tunnel and strengthen the interaction. Also, Touber and Sandham [30] provided new insight about low-frequency unsteadiness regarding turbulent SWBLI by means of LES. The data were used to derive an analytical model based on a stochastic ordinary differential equation, starting from Navier–Stokes equations. The model describes the coupled shock/boundary-layer system as a first-order low-pass filter.

In terms of flow control, many techniques are used to prevent separation of boundary layers, such as vortex generators (Lin and Howard [31]), passive cavities (Raghunathan [32]), streamwise slots (Smith and Babinsky [33]), or microramps (Lapsa [34] and Lee et al. [35]). For instance, Lee et al. [35] used microvortex generators for shock/boundary-layer interaction control. A Mach 3 turbulent boundary layer at moderate Reynolds number with shock impinging has been considered. The experiments were coupled with a monotone-integrated large-eddy simulation technique to study the dynamics of the shock/turbulent structures interaction and to predict the behavior of the primary vortices formed by the microramp. The effects of microramp size and location were also studied. Under certain conditions, a reduction in the displacement thickness of the boundary layer (of as much as 30%) was observed with a decrease in the size of the separated zone.

The present work focuses on the use of large-eddy simulations for the study of an oblique shock interacting with turbulent boundary layer over an adiabatic flat plate (see Fig. 1). To provide more insight into the computed results, the experimental data provided by Deleuze [36], Laurent [37], and more recently by Debiève and Dupont [24] are used to study the unsteady aspects of the 3-D SWBLI, with particular emphasis on the origin of the low-frequency oscillations associated with wall pressure fluctuations. The paper also briefly addresses the important question of the three-dimensionality of the flow in the presence of sidewalls, and the possible effect of the spanwise confinement on the flow organization together with the associated low-frequency unsteadiness.

II. Methodology

A. Large-Eddy Simulation

Consider the low-pass-filtered Navier–Stokes equations

$$\partial_t \bar{\rho} + \partial_j(\bar{\rho}\tilde{u}_j) = 0$$
$$\partial_t(\bar{\rho}\tilde{u}_i) + \partial_j(\bar{\rho}\tilde{u}_i\tilde{u}_j) + \partial_i\bar{\rho} = \partial_j\breve{\sigma}_{ij} - \partial_j\tau_{ij}$$
$$\partial_t(\bar{\rho}\breve{E}) + \partial_j(\bar{\rho}\breve{E}\tilde{u}_j) + \partial_i(\tilde{u}_i\bar{\rho}) = \partial_j(\tilde{u}_i\sigma_{ij}) - \partial_j\breve{q}_j - \partial_j(\tilde{u}_i\tau_{ij}) - \partial_j\mathcal{Q}_j$$

where $\bar{\rho}$, $\tilde{u}_i$, $\bar{p}$, and $\tilde{T}$ are the filtered density, velocity, pressure, and temperature, respectively. Unlike the "bar" and the "tilde," the "breve" symbol does not denote a filter operation but indicates that the quantity is based on primitive filtered variables. Thus $\breve{E}$ refers to the resolved total energy, which is not equal to the filtered total energy. The resolved viscous stress tensor $\breve{\sigma}_{ij}$ and the heat flux $\breve{q}_j$ are defined as

$$\breve{\sigma}_{ij} = 2\mu(\tilde{T})(\tilde{S}_{ij} - \partial_k\tilde{u}_k\delta_{ij}/3),$$
$$\tilde{S}_{ij} = (\partial_j\tilde{u}_i + \partial_i\tilde{u}_j)/2,$$
$$\breve{q}_j = -\lambda(\tilde{T})\partial_j\tilde{T}$$

where $\mu(\tilde{T})$ and $\lambda(\tilde{T})$ are the viscosity and thermal conductivity corresponding to the filtered temperature $\tilde{T}$. The low-pass filtering generates several unclosed terms; most of these are neglected, except for the subgrid stress τ_{ij} and the subgrid heat flux $\mathcal{Q}_j$, which are modeled using an eddy-viscosity hypothesis as

$$\tau_{ij} = -\mu_t(\partial_j\tilde{u}_i + \partial_i\tilde{u}_j - \partial_k\tilde{u}_k 2\delta_{ij}/3) + k_{\text{sgs}}2\delta_{ij}/3,$$
$$\mathcal{Q}_j = -\kappa_t\partial_j\tilde{T}, \qquad \mu_t = C_d\Delta^2\bar{\rho}|\tilde{S}|,$$
$$k_{\text{sgs}} = C_I\Delta^2\bar{\rho}|\tilde{S}|^2, \qquad \kappa_t = c_p\mu_t/Pr_t$$

The modeling parameters C_d, C_I, and Pr_t are determined through the dynamic procedure of Germano et al. [38], Lilly [39], and Moin et al. [40] with filtering and averaging in the homogeneous (periodic) direction. Δ is the filter width associated with the wavelength of the smallest scale retained by the filtering operation.

B. Numerical Method

In addition to the subgrid-scale modeling, another issue of the LES technique is the choice of the numerical method. Modern low-dissipative high-order methods, based on Riemann solvers and high-order weighted essentially nonoscillatory (WENO) interpolations, are now generally regarded as offering an accurate and stable numerical framework. However, several studies [41,42] indicated that these high-order shock-capturing schemes are still much too dissipative to capture fine-scale turbulence fluctuations. This has encouraged the hybridization between spectral or high-order compact schemes and high-resolution shock-capturing methods, in which a flow sensor is used to switch to shock-capturing methods at discontinuities. Adams and Shariff [43] have first proposed an adaptive hybrid compact essentially nonoscillatory (ENO) scheme, coupling a compact upwind scheme with a fifth-order ENO scheme

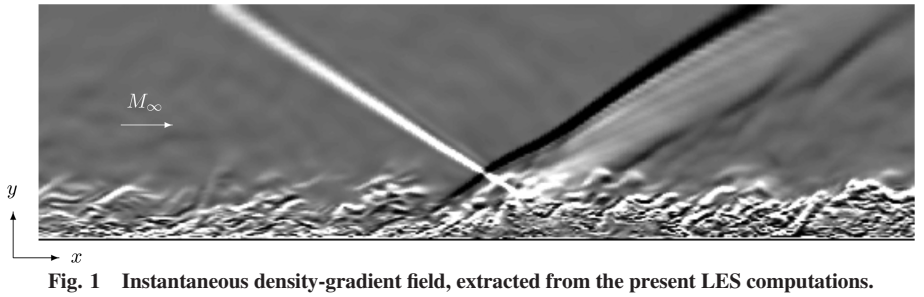

Fig. 1 Instantaneous density-gradient field, extracted from the present LES computations.

that is active only near discontinuities. Later, the method was extended by Pirozzoli [44] to a fully conservative formulation based on hybridizing a fifth-order compact upwind numerical flux with a seventh-order WENO flux, the switch being based on the local density gradient. Further improvements to the hybrid WENO were introduced by Ren et al. [45], Hill and Pullin [46], Pantano et al. [47], and Chao et al. [48].

In this study, a fifth-order WENO scheme combined with a centered fourth-order scheme is used to calculate the convective fluxes, via the selective Ducros' sensor. The inviscid numerical flux $\hat{f}$ is computed between grid points through the blended formula

$$\hat{f} = \varsigma \hat{f}^{w} + (1-\varsigma)\hat{f}^{c}$$

where $\hat{f}^{w}$ and $\hat{f}^{c}$ are the fluxes interpolated through fifth-order WENO and fourth-order central (nondissipative) interpolation, respectively. The switching-function ς is determined for each grid point once per time step by the following algorithm. It is defined as one if

$$|\partial_k u_k| > \phi_c \sqrt{(\partial_k u_k)^2 + \Omega^2} \tag{1}$$

and zero otherwise; Ω is a low-pass-filtered vorticity magnitude and ϕ_c is a given threshold for which the solution is considered as nonsmooth and the WENO scheme is applied. For stability reasons, a threshold value of $\phi_c \approx 0.17$ is used. The shock sensor given by Eq. (1) marks regions of strong compression and avoids marking weak acoustic waves in irrotational regions. To avoid applying the central scheme for $\hat{f}^{c}$ across shocks, it is necessary to expand the region shock to two neighboring points.

Viscous terms are discretized using a centered fourth-order accurate scheme, whereas an explicit third-order Runge–Kutta method of Shu and Osher [49] is used for time integration. Concerning the inflow boundary conditions, an existing method for the generation of unsteady compressible turbulent boundary layers, based on a digital filter approach, is used. The main advantage of this method over the recycling/rescaling approach or the forced laminar-to-turbulent transition technique is to allow the simulation to generate its own coherent inflow data without introducing any particular mode into the computational domain (in particular, the low-frequency one), which may interact with the shock/boundary-layer system. The detailed procedure of this method can be found in Touber [50].

III. Results and Discussion

A. Supersonic Incoming Boundary Layer

We first report some of the characteristics of the supersonic incoming boundary layer (in the absence of interacting shock), which evolves at $M_\infty = 2.28$ and has a momentum-thickness Reynolds number of $R_{e_\theta} \simeq 5350$. The size of the computational domain is $L_x \approx 15\delta_{\text{in}}$, $L_y \approx 6.5\delta_{\text{in}}$, $L_z \approx 5\delta_{\text{in}}$, where $\delta_{\text{in}} = 10.83$ mm is the incoming boundary-layer thickness. Note that the spanwise length was varied from $\sim\delta_{\text{in}}$ (narrow domain) to $5\delta_{\text{in}}$ (wide domain) to cover roughly half of the wind-tunnel extent. The two-point autocorrelation coefficients in the homogeneous direction (z) for both cases (narrow and wider domains) are examined. Results (not presented here for brevity) show that the decorrelation of velocity and pressure fluctuations is achieved over a distance of $L_z/2$ for both narrow and wide domains, which indicates that the turbulence dynamics are not inhibited. Basically, in terms of turbulence statistics, no significant differences were found between the two different domain extents. This suggests that the narrow-span LES is, in general, sufficient to resolve most of the features occurring in boundary layers. However, as will be discussed later, the variation of the spanwise length may significantly affect the predicted interaction lengths and the associated low-frequency unsteadiness. In what follows, only results of the wider domain will be presented and discussed. In this case, the mesh contains 10^7 grid points and is stretched in the wall-normal direction with more clustering in the boundary layer. In wall units, the closest grid point to the wall is at $\Delta y^{+}_{\text{min}} \simeq 1$ (the superscript $+$ indicates usual normalization by the friction velocity, with $y^{+} = \rho_w y u_\tau/\mu_w$, where μ_w and ρ_w are the dynamic viscosity and the density at the wall, respectively). In the streamwise and spanwise directions, the mesh resolution gives cell sizes in wall units of $\Delta x^{+} = 40$ and $\Delta z^{+} = 16$, respectively.

Regarding the boundary conditions, the flow is first assumed to be homogeneous in the spanwise direction, so that periodic boundary conditions are retained. The examination of the instantaneous three-dimensional isovorticity field shows that the boundary layer is fully developed and self-sustaining. Also, the simulation reveals the appearance of large-scale motion in the outer region of the boundary layer, dominated by the entrainment process. These large-scale structures are particularly active near the edge of the boundary layer, where they remain coherent long enough so that they are strongly responsible for the intermittency of the boundary layer and its growth rate. The reported turbulence statistics are examined to evaluate their consistency with both DNS [51] and measurements [36,37]. They are based on time averaging of the instantaneous three-dimensional fields that are extracted from a time series covering 200 characteristic times, $\tau_c = \delta_{\text{in}}/U_\infty$. As shown in Fig. 2, the LES results match well with both DNS and experimental data. The DNS of Pirozzoli et al. [51] concerns a spatially developing supersonic adiabatic flat plate boundary-layer flow at $M_\infty = 2.25$ and $Re_\theta \approx 4000$, which has become a standard test for evaluation of LES and DNS simulations. The numerical algorithm is based on a mixed WENO compact-difference method and the finest mesh used was $2065 \times 56 \times 255$ grid points with a spatial resolution of $\Delta x^{+} = 13.9$, $\Delta y^{+} = 0.97$, and $\Delta z^{+} = 6.56$. An upstream region of blowing and suction is introduced to induce laminar-to-turbulent transition. Detailed results of the first- and second-order turbulent statistics were provided and the assessment of the validity of Morkovin's hypothesis was made. It is worth noting that the near-wall behavior of the subgrid viscosity is well recovered ($\mu_t \sim y^{+3}$), showing that the current subgrid modeling, which does not incorporate any information related to the location of the solid walls, is well suited for the simulation of bounded turbulent flows.

B. Shock/Boundary-Layer Interaction

Considering the shock/boundary-layer interaction problem, the computations are performed based on the test case studied experimentally by the Institut Universitaire des Systèmes Thermiques Industriels group in Marseille, France [36,37]. The shock generator has an angle of $\theta = 8$ deg, which corresponds to an oblique shock of 32.41 deg inclination at Mach 2.28. The incoming boundary condition is extracted from the data of the spatially developing boundary layer discussed in the previous section. The size of the computational domain is nearly the same, except for an extension made in both x and y directions to cover both the interaction zone and the relaxation region. This is to avoid a possible confinement of the shock system in the cross-streamwise direction. An extensive grid refinement was performed to achieve an improvement in the predicted flow both with respect to the separation and the reattachment positions. The final mesh contained $N_x \times N_y \times N_z = 375 \times 160 \times 461$ points, covering $L_x \times L_y \times L_z = 20 \times 10 \times 5\delta_{\text{in}}$. As shown in Table 1, the range of domain size and grid resolutions used in the present study fits well with the previous LES investigations for similar flow parameters.

C. Turning Off the Subgrid Model Near Shocks

It is important to notice that the presence of the shock wave poses a particular problem in LES. Indeed, the subgrid viscosity ratio μ_t/μ may exhibit high values near discontinuities, even outside of the boundary layer. This result is not surprising because the amount of subgrid viscosity evolves proportionally to the second invariant of the deformation tensor. Thus, the resolved turbulence can be artificially damped when crossing the shock. To overcome this problem, the subgrid model was used only in the region of the flow where the centered scheme is active. In other words, the switching function ς is used to deactivate the subgrid model near shocks, simply by setting τ_{ij} and $\mathcal{Q}_j$ to zero. Note that this does not

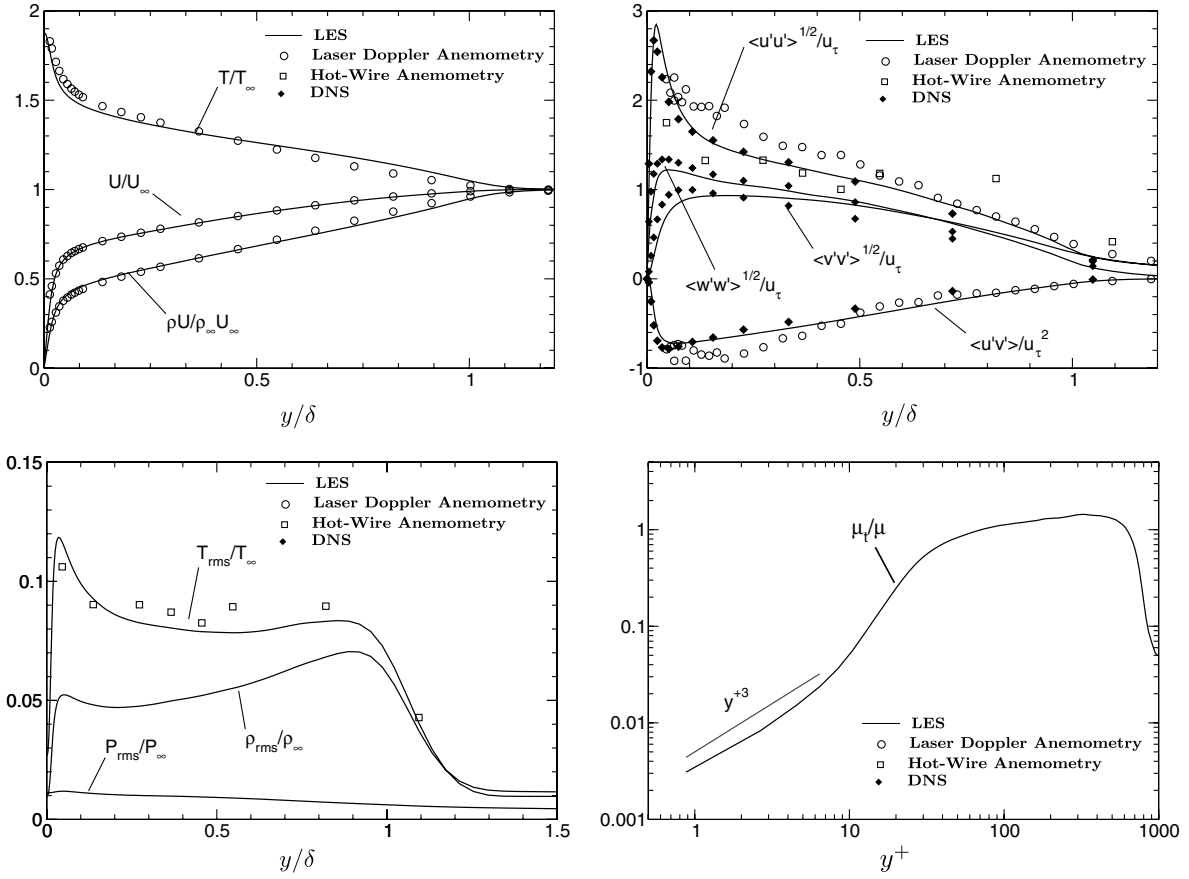

Fig. 2 Wall-normal distributions of first- and second-order turbulence statistics of the incoming boundary layer [51].

compromise the conservation of momentum or total energy, because these terms appear inside divergences. Moreover, note that this method can be used with any subgrid model and not just those of eddy-viscosity type. We should note that this simplistic approach should be modified for highly corrugated shocks, where some type of shock-confining filters should be used.

1. *Instantaneous Structures and Mean Properties*

The instantaneous isosurface of the Q vortex-identification criterion, reported in Fig. 3, reveals the existence of complex organized motion in the outer part of the boundary layer, as well as in the interaction zone, which is characterized by the occurrence of large-scale structures that exhibit a highly intermittent character. The interaction region is characterized by "intermittent detachment" with scattered spots of instantaneous flow reversal throughout the interaction zone, and by the formation of a turbulent mixing layer, with associated unsteady release of vortical structures (see Fig. 1). At the interaction point, the incident shock bends toward the wall while penetrating the boundary layer and then is reflected back through the sonic line. The time-averaged flowfield exhibits a small recirculation bubble close to the wall, which is induced by the impingement of the incident shock onto the separated boundary layer. Later, the formation of an expansion fan followed by a series of compression

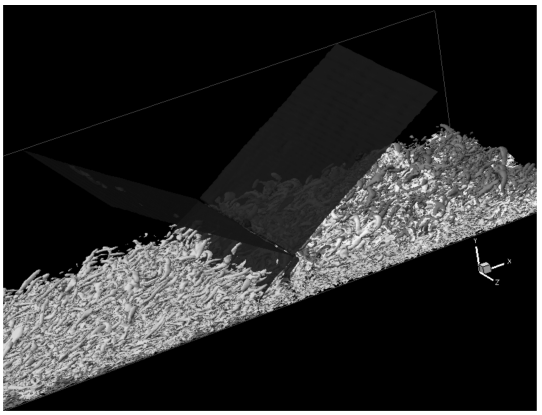

Fig. 3 Instantaneous isosurface of the second invariant of the velocity gradient tensor $Q = 0.01Q_{\max}$ colored by the density field.

waves helps the boundary layer to reattach to the wall and to relax further downstream. Figure 3 also demonstrates that the postseparation shear layer contains a coherent motion associated with the Kelvin–Helmholtz-like vortices (some of them are visible on

Table 1 Simulation parameters (grid resolution and domain size) of the oblique shock impinging on a turbulent boundary-layer problem

Case	M_∞	R_{e_θ}	$L_x \times L_y \times L_z$	$N_x \times N_y \times N_z$	Δx^+	$\Delta y^+_{\min}$	Δz^+
DNS (Pirozzoli and Bernardini [55])	2.28	2300	$80\delta \times 12\delta \times 6\delta$	$3841 \times 344 \times 261$	5.6	0.93	6.6
LES (Morgan et al. [56])	2.08	2188	$25\delta \times 10\delta \times 5\delta$	$471 \times 155 \times 160$	30	1	16
LES (Touber and Sandham [57])	2.30	5000	$20\delta \times 4\delta \times 4.7\delta$	$451 \times 151 \times 110$	33	1.3	12
LES-L4 (Pirozzoli et al. [54])	2.28	5000	$60\delta \times 10\delta \times 4\delta$	$929 \times 252 \times 110$	43	1.2	24
LES (Garnier and Sagaut [27])	2.30	5346	$17\delta \times 6.5\delta \times 0.7\delta$	$255 \times 151 \times 55$	50	1	18
LES (current study)	2.28	5350	$20\delta \times 10\delta \times 5\delta$	$375 \times 160 \times 461$	40	1	16

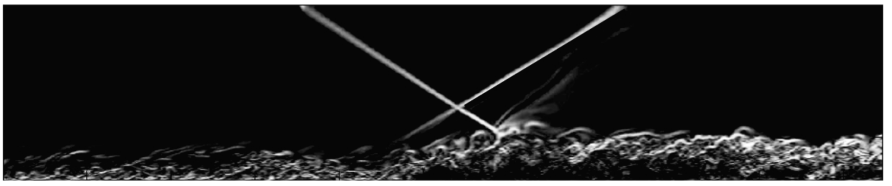

Fig. 4 Instantaneous vorticity field.

Fig. 4). This organized motion contributes directly to the turbulence level in the shear layer as well as interacts sensitively with the temporal variation of the separation process. The computed mean and fluctuating velocities at several measurement locations are shown in Fig. 5. Also, the wall pressure and the skin friction coefficient are plotted in Fig. 6. Throughout the interaction region, the computation shows, in general, close agreement with the experiments. Figure 7 shows that the shock sensor given by Eq. (1) is capable of selectively isolating compressed regions (shocks) from purely turbulent flows.

2. *Strong Reynolds Analogy*

The objective behind the analysis of the strong Reynolds analogy (SRA) is to test the departure from the common assumption in the specific case of shock/boundary-layer interaction, and to verify the applicability of Morkovin's hypothesis. Reynolds analogies in supersonic flows imply that the total temperature fluctuations are negligible and the turbulent Prandtl number is one. In particular, this yields to the following relations:

$$\mathrm{SRA} = \frac{\sqrt{\langle T'T'\rangle}/\tilde{T}}{(\gamma-1)\langle M\rangle^2\sqrt{\langle u'u'\rangle}/\tilde{u}} \approx 1,$$
$$R_{u'T'} = \frac{\langle u'T'\rangle}{\sqrt{\langle u'^2\rangle\langle T'^2\rangle}} \approx -1 \tag{2}$$

where $\langle M\rangle = \langle u\rangle/\langle c\rangle$ is the local Mach number, and where $\langle\cdot\rangle$ implies time and space averages. As shown in Fig. 8 (right), the relations (2) are not valid in the boundary layer as well as in the interaction and the relaxation regions. For instance, the value of the measured correlation coefficient $-R_{u'T'}$ is less than unity ($\approx$0.85) in most of the flow. In addition, DNS data of supersonic boundary layers [51,52] have shown that this coefficient remains close to 0.60 throughout most of the boundary layer and exhibits a maximum value of 0.84 when approaching the wall. In this case, both DNS and LES reproduce the same trend, except in the outer part of the boundary layer where the correlation coefficient falls to 0.45 for LES. As suggested by Gaviglio [53], discrepancies observed between

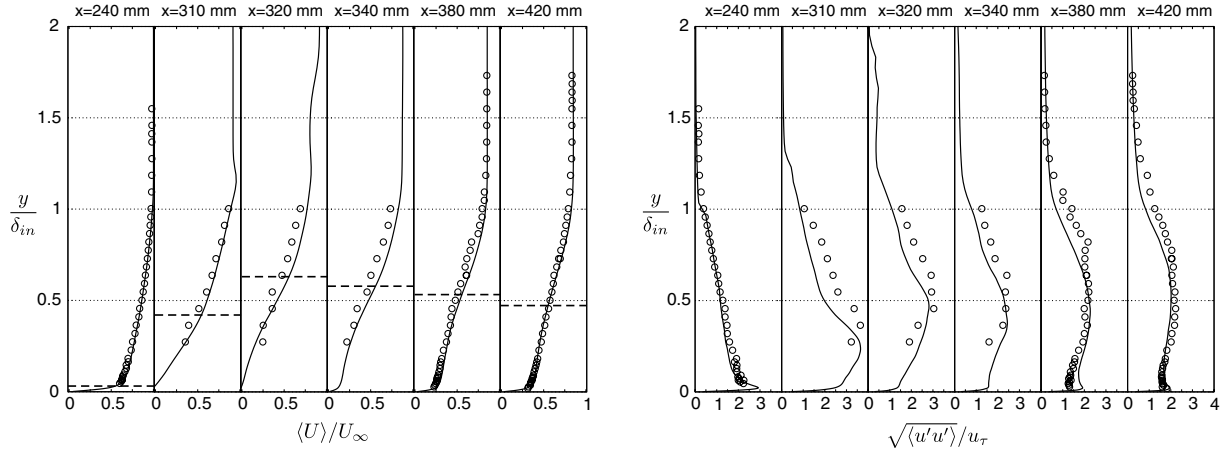

Fig. 5 Longitudinal mean and fluctuating velocity profiles vs. y/δ_{in} in the upstream boundary layer and along the interaction region. Solid line, LES; open circle, Laser-Dopler Anemometry (LDA); dashed line, sonic line.

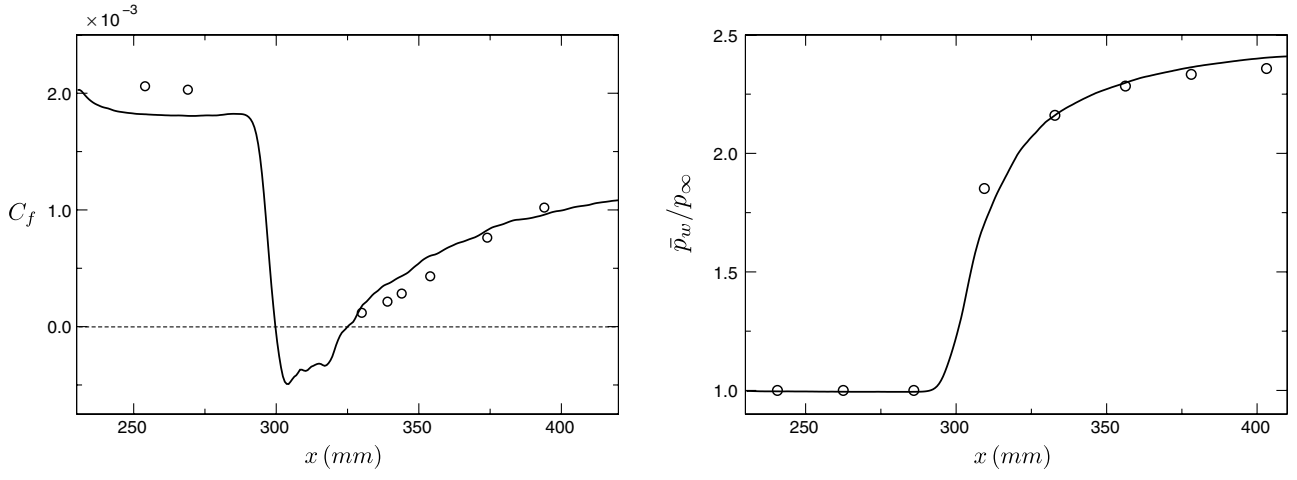

Fig. 6 Wall quantities, (Left) Skin-friction coefficient. (Right) Normalized wall-pressure distribution. Solid line, LES; open circle, experiments.

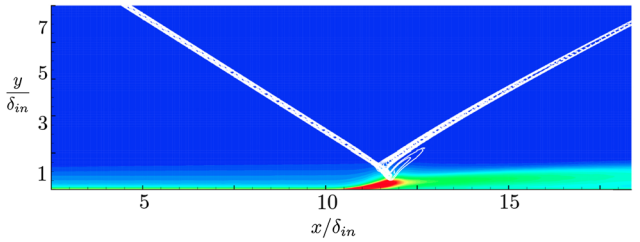

Fig. 7 Two-dimensional mean distribution showing rms of the wall-normal velocity fluctuations in filled contours and the shock detector in solid white lines.

experiments and simulations may be due to a difference in the magnitude of the acoustic field, which is not the same in the computation as in the blowdown wind tunnel. Furthermore, these results confirm that the fluctuations of the total temperature are not negligible and the SRA is no longer valid either in the boundary layer or in the postshock interaction region.

3. *Analysis of Shock-Wave/Boundary-Layer Interaction Unsteadiness*

The problem of shock unsteadiness at low frequency, relative to the higher characteristic frequency of the incoming turbulent boundary layer, is somehow related to the dynamics of the separated bubble, which pulsates the whole shock system and causes global unstable movement, generally leading to strong expansions and contractions of the flowfield in a breathing motion. Also, the boundary-layer separation gives rise to a detached shear layer that convects the perturbations far downstream. The associated shedding phenomenon is known to generate strong coupling between the shock region and the downstream relaxation zone. Figure 9 (left) displays contours of rms pressure, $p_{\text{rms}} = \sqrt{\overline{p'p'}}$. It can be seen that the amplification of pressure fluctuations is much more important in the interaction zone and in the downstream relaxation region (6–7% of $P_{\infty,\text{in}}$) compared with the upstream boundary layer, which exhibits a lower level (2% of $P_{\infty,\text{in}}$). This behavior is clearly visible in the wall-pressure distribution (Fig. 9, right), which shows higher values of $\sqrt{\overline{p'p'}}$ near the reflected shock. In accordance with recent experimental observations [6], one can attribute this amplification to the unsteady behavior of the separated shock system. In the same way, the foot of the incident shock, supported by the sonic line, exhibits strong fluctuations, which possibly result from oscillations of the recirculation bubble, as mentioned before. Note that the current p_{rms} prediction shows good agreement with the LES-L4 of Pirozzoli et al. [54], which is a full-scale LES made in attempt to match the experimental conditions. The size of the computational domain as well as the grid resolution are given in Table 1 and the flow solver is described in [55]. Note that the origin of the x axis corresponds to the beginning of the interaction zone, whose length is $L \simeq 3\delta_{\text{in}}$, with a corresponding separation length $L_{\text{sep}} \simeq 3.14\delta_{\text{in}}$.

Power spectral density (PSD) of wall-pressure fluctuations is shown in Fig. 10 along with the longtime wall-pressure history. The field represents spatial distribution of iso-PSD (x, $\log(F)$) normalized by its local integral $G_n(F)$. This normalization has the advantage of better highlighting the contribution of each frequency at a given coordinate x, with

$$\int_0^\infty G_n(f)\,\mathrm{d}f|_x = 1$$

The average wall-pressure profile is also reported in the same figure to help localize the compression waves acting on the shock foot. An energy accumulation at low frequencies is observed at $295 < x < 310$ mm (including a part of the separated zone), which reveals the

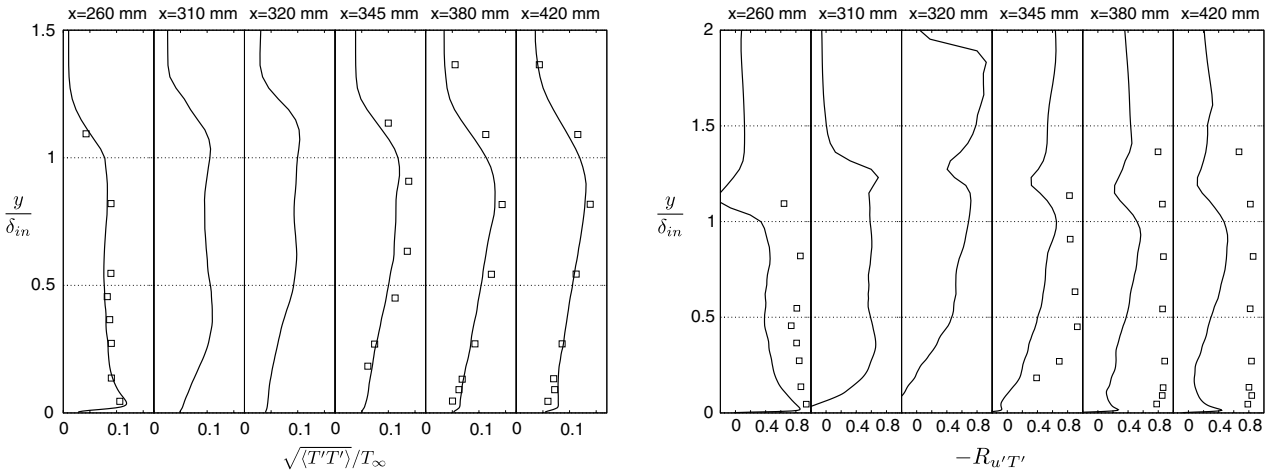

Fig. 8 Temperature fluctuation and $-R_{u'T'}$ correlation. Solid line, LES; open box, experiments (hot wire anemometry).

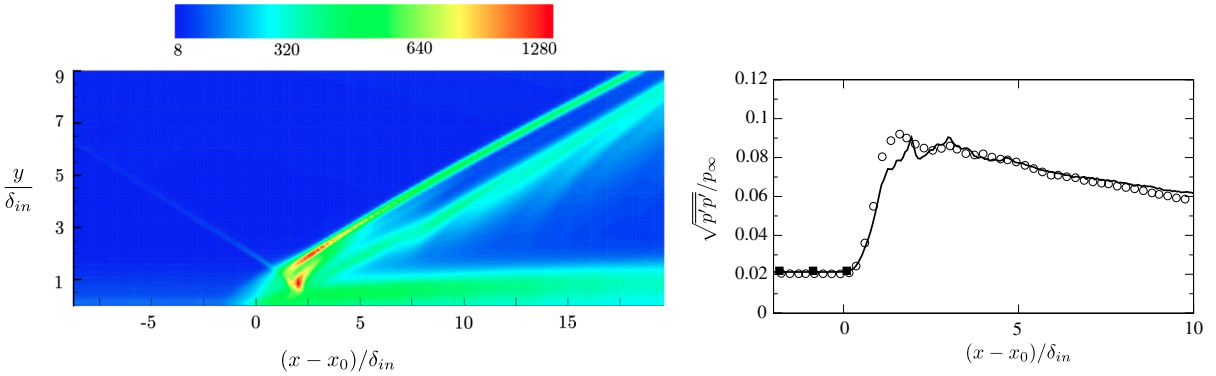

Fig. 9 rms pressure, (Left) plot of $\sqrt{\overline{p'p'}}$ (Pa), (Right) longitudinal distribution of rms wall pressure normalized by the reference static pressure. Solid line, present LES; open circle, LES from [54]; filled square, ratio of wall rms from [58].

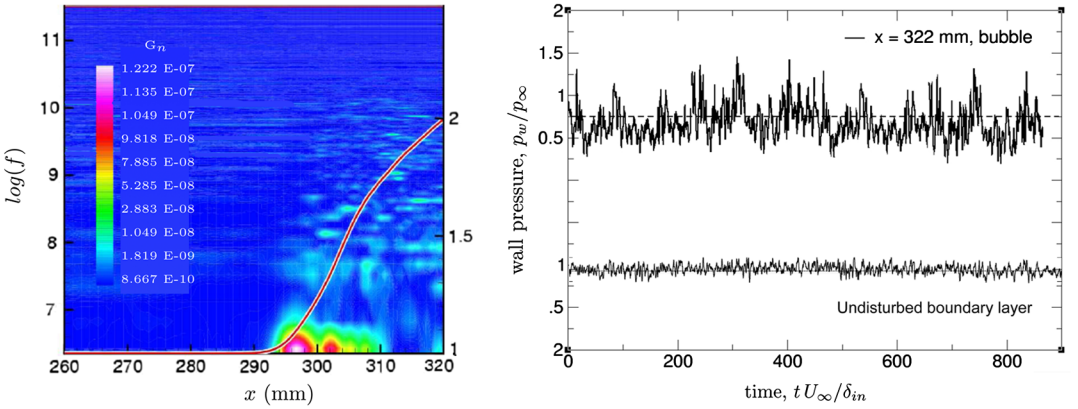

Fig. 10 (Left) PSD of wall-pressure fluctuations normalized using its local integral, plotted with the mean profile of the wall pressure (solid line). (Right) Instantaneous long time wall-pressure signals.

existence of a low-frequency movement of the reflected shock (<1 kHz and $S_t \approx 0.02$. Here, the Strouhal number is defined as $S_t = fL_{\text{sep}}/U_\infty$).

This observation is in agreement with experimental investigations, which emphasizes a dominant frequency, associated with the shock movement, of 350 Hz ($S_t \approx 0.01$). It is worth noticing that the highest energy contribution is located at the beginning of the separation zone ($295 < x < 300$ mm), whereas energies associated with frequencies lower than 1 kHz are very weak in the upstream boundary layer, as well as in the central part of the recirculation zone ($x = 315$ mm). It seems, however, that low-frequency phenomena reappear at the end of the recirculation zone ($x = 320$ mm). For further investigations of shock oscillations, PSD of surface pressure fluctuations, conditioned by the average shock position, at the outer part of the boundary layer ($x = 322$ mm and $y = 16.8$ mm, for $y^+_{\text{in}} = 1150$), are examined. Results (not shown here for concision) show clearly that high energies are associated with frequencies lower than 1 kHz, confirming experimental evidence of low-frequency shock oscillations. PSD signals of $\rho u'$ are also analyzed. Again, we notice an energy accumulation associated with a low-frequency unsteadiness of the recirculation bubble (<1 kHz), featuring similarities with the movement of the reflected shock.

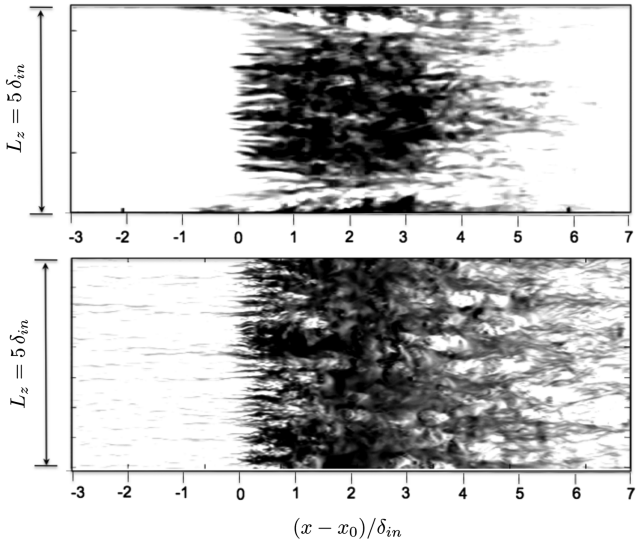

Fig. 11 Instantaneous snapshot of u'/U_∞ at $y^+ = 10$ with two different spanwise boundary conditions; (top) slip condition, (bottom) periodic condition.

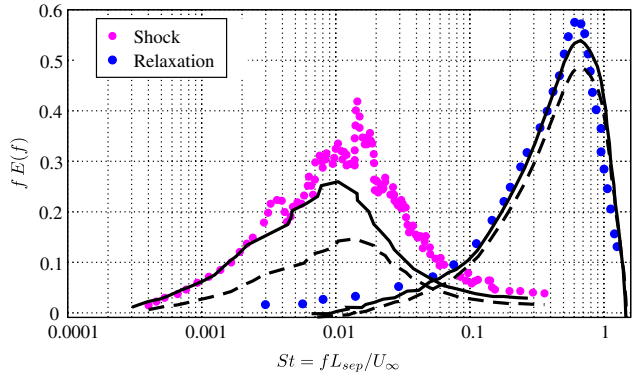

Fig. 12 Premultiplied PSD. Solid line, LES-slip-walls, with the data taken at the centerline of the computational domain, $L_z/2$; dashed line, LES periodic; filled circles, experimental data [28].

Finally, Fig. 11 highlights the importance of the spanwise boundary conditions on the global flow organization in general and on the interaction zone and the reversal flow in particular. Because of the limitation on the CPU time and computer memory, the boundary layer on the sidewalls was not solved. Instead, lateral slip boundaries with reflecting boundary conditions were employed. The idea behind this is to confine the flow, by keeping the total mass flow constant. To help stabilize the flow, the turbulent velocity fluctuations in the spanwise direction were damped and boundary-layer-like profiles are specified at the inlet boundary along the sidewalls to avoid singularity. The main difference between the two computations is observed downstream of the interaction, where the bubble contour of the confined case exhibits two small near-wall vortices, which closely resemble the experimental results. In addition, one must recall that the shape of the separation bubble depends on the spanwise length and, therefore, large streamwise structures may affect the shock front by producing spanwise wrinkles. The sidewall vortices are found to reduce the effective spanwise section and strengthen the interaction. It was also found that the low-frequency energy content is greater in the confined case compared with the periodic one (see Fig. 12). However, the relation between the corner-flow unsteadiness and the low-frequency motion of the main separation bubble is still an open question.

IV. Conclusions

The major properties of the flow occurring when an incident oblique shock interacts with a flat plate turbulent boundary layer have been investigated using large-eddy simulations. The study mainly focuses on the unsteady aspects of the interaction, with particular emphasis on the origin of the low-frequency oscillations associated with wall-pressure fluctuations. It has been shown that the present large-eddy simulation (LES) does capture the important dynamics of this interaction, namely, the frequency of the most energetic low-frequency unsteadiness and the bandwidth of the low-frequency content. The simulation also highlights the effect of sidewalls on the flow characteristics, including the shock structure, the separated flow region, and the low-frequency content associated with the

wall-pressure fluctuations. In this study, full validation of the numerical data has been achieved through systematic computational fluid dynamics/experiment comparison. This verification step is important because it helps to provide an estimate of the accuracy of the modeling. In this regard, it has been shown that the LES accurately predicts the mean temperature and density profiles, wall pressure, root mean square of velocity, temperature fluctuations, and Reynolds shear stress profiles. In agreement with both direct numerical simulation and experimental data, this study also shows that the streamwise velocity component and the temperature are weakly anticorrelated ($-R_{u'T'} \approx 0.5$). Experimental evidence suggests, however, a higher value of the correlation coefficient than the one found in the simulation. In this case, fluctuations of the total temperature are not negligible and the strong Reynolds analogy is not valid. Finally, oscillations of the reflected shock occurring at low frequencies are observed, in agreement with previous numerical and experimental investigations. Simulations reveal the presence of such frequencies mainly downstream of the shock and near the recirculation bubble. The fact that the low frequencies of the shock/bubble system persist, even in the absence of upstream low-frequency forcing, would therefore seem to suggest that they are not due to a low-pass filtering effect. Rather, they must be a consequence of the intrinsic dynamics of the system (in the sense of a global mode). Although basic understanding of flow physics of this interaction has been achieved through different numerical and experimental investigations, substantial additional research in full 3-D shock-wave turbulent boundary-layer interactions is still needed. In particular, if the structure of the interaction is strongly affected by the lateral walls, the shock will certainly accommodate with this complex three-dimensional organization, and spanwise shock oscillations will develop with different frequencies and wavelengths. Consequently, full characterization of the flowfield should be attempted by means of 3-D simulations, including lateral-wall effects, in conjunction with a global stability analysis that can be conducted in parallel.

Acknowledgments

This research is supported by the Center for Turbulence Research, Stanford University. Part of this work was performed using High-Performance Computing (HPC) resources from Grand Equipement National de Calcul Intensif (GENCI) [Centre de Calcul Recherche et Technologie (CCRT)/Centre Informatique de l'Enseignement Supérieur (CINES)/Institut de Développement et des Ressources en Informatique Scientifique (IDRIS)] (grant 2010-0211640). The author gratefully acknowledges stimulating discussions during the Center for Turbulence Research (CTR) Summer Program with S. K. Lele, J. Larsson, B. Morgan, and J. Nichols from Stanford University, USA and S. Pirozzoli and M. Bernardini from University of Roma "La Sapienza," Italy. Special thanks to I. Bermejo-Moreno from CTR for his valuable remarks and helpful comments on the early manuscript draft. The author also acknowledges fruitful e-mail exchanges and discussions with E. Touber from Imperial College, United Kingdom, who kindly supplied large-eddy simulation data for a preliminary validation of the current simulations.

References

[1] Nguyen, A. T., Deniau, H., Girard, S., and Alziary deRoquefort, T., "Wall Pressure Fluctuations in an Over-Expanded Rocket Nozzle," *38th AIAA/ASME/SAE/ASEE Joint Propulsion Conference and Exhibit*, Paper 2002-4001, 2002.

[2] Girard, S., "Etude des Charges Latérales dans une tuyère Supersonique Surdétendue," Ph.D. Thesis, University of Poitiers, Poitiers, France, 1999.

[3] Salmon, J. T., Bogar, T. J., and Sajben, M., "Laser Doppler Velocimeter Measurements in Unsteady, Separated Transonic Diffuser Flows," *AIAA Journal*, Vol. 21, No. 12, 1983, pp. 1690–1697. doi:10.2514/3.8311

[4] Sajben, M., Bogar, T. J., and Kroutil, J. C., "Forced Oscillation Experiments in Supercritical Diffuser Flows," *AIAA Journal*, Vol. 22, No. 4, 1984, pp. 465–474. doi:10.2514/3.8423

[5] Kim, J., and Sung, H. J., "Wall Pressure Fluctuations in a Turbulent Boundary Layer over a Bump," *AIAA Journal*, Vol. 44, No. 7, 2006, pp. 1393–1401. doi:10.2514/1.6519

[6] Dupont, P., Haddad, C., and Debiève, J.-F., "Space and Time Organization in a Shock-Induced Separated Boundary Layer," *Journal of Fluid Mechanics*, Vol. 559, 2006, pp. 255–277. doi:10.1017/S0022112006000267

[7] Erengil, M. E., and Dolling, D. S., "Unsteady Wave Structure Near Separation in a Mach 5 Compression Ramp Interaction," *AIAA Journal*, Vol. 29, No. 5, 1991, pp. 728–735. doi:10.2514/3.10647

[8] Ganapathisubramani, B., Clemens, N. T., and Dolling, D. S., "Effects of Upstream Boundary Layer on the Unsteadiness of Shock-Induced Separation," *Journal of Fluid Mechanics*, Vol. 585, Aug. 2007, pp. 369–394. doi:10.1017/S0022112007006799

[9] Dolling, D. S., "Fifty Years of Shock-Wave/Boundary-Layer Interaction Research: What Next?," *AIAA Journal*, Vol. 39, 2001, pp. 1517–1531. doi:10.2514/2.1476

[10] Settles, G. S., and Dolling, D. S., "Swept Shock Wave/Boundary Layer Interactions: Tutorial and Update," AIAA Paper 90-0375, 1990.

[11] Délery, J., Marvin, J. G., "Shock-Wave Boundary Layer Interactions," AGARDograph 280, 1996.

[12] Dolling, D., and Dussauge, J. P., "Fluctuating Wall-Pressure Measurements," AGARDograph 315, NATO, Neuillys/Seine, 1989.

[13] Andreopoulos, J., and Muck, K., "Some New Aspects of the Shock-Wave/Boundary Layer Interaction," *Journal of Fluid Mechanics*, Vol. 180, No. -1, 2006, pp. 405–428. doi:10.1017/S0022112087001873

[14] Andreopoulos, Y., Agui, J., and Briassulis, G., "Shock Wave-Turbulence Interactions," *Annual Review of Fluid Mechanics*, Vol. 32, No. 1, 2000, pp. 309–345. doi:10.1146/annurev.fluid.32.1.309

[15] Unalmis, O., and Dolling, D., "Experimental Study of Causes of Unsteadiness of Shock Induced Turbulent Separation," *AIAA Journal*, Vol. 36, 1998, pp. 371–378. doi:10.2514/2.373

[16] Beresh, S. J., Clemens, N. T., and Dolling, D. S., "Relationship Between Upstream Turbulent Boundary-Layer Velocity Fluctuations and Separation Shock Unsteadiness," *AIAA Journal*, Vol. 40, No. 12, 2002, pp. 2412–2422. doi:10.2514/2.1609

[17] Hou, Y., Clemens, N., and Dolling, D., "Wide-Field PIV Study of Shock-Induced Turbulent Boundary Layer Separation," AIAA Paper 2003-0441, 2003.

[18] Adrian, R. J., Meinhart, C. D., and Tomkins, C. D., "Vortex Organization in the Outer Region of the Turbulent Boundary Layer," *Journal of Fluid Mechanics*, Vol. 422, Nov. 2000, pp. 1–53. doi:10.1017/S0022112000001580

[19] Humble, R., Elsinga, G., Scarano, F., and van Oudheusden, B., "Three-Dimensional Instantaneous Structure of a Shock Wave/Turbulent Boundary Layer Interaction," *Journal of Fluid Mechanics*, Vol. 622, 2009, pp. 33–62. doi:10.1017/S0022112008005090

[20] Wu, M., and Martin, M. P., "Analysis of Shock Motion in STBLI Using Direct Numerical Simulation Data," *Journal of Fluid Mechanics*, Vol. 594, 2008, pp. 71–83.

[21] Dolling, D., and Smith, D., "Unsteady Shock Induced Separation in Mach 5 Cylinder Interactions," *AIAA Journal*, Vol. 27, No. 12, 1989, pp. 1598–1706.

[22] Gramman, R. A., and Dolling, D. S., "Detection of Turbulent Boundary Layer Separation Using Fluctuating Wall Pressure Signals," *AIAA Journal*, Vol. 28, 1990, pp. 1052–1056. doi:10.2514/3.25164

[23] Hou, Y. X., Unalmis, O. H., and Bueno, P. C., "Effects of Boundary-Layer Velocity Fluctuations on Unsteadiness of Blunt-Fin Interactions," *AIAA Journal*, Vol. 42, No. 12, 2004, pp. 2615–1219.

[24] Debiève, J. F., and Dupont, P., "Dependence Between the Shock and the Separation Bubble in a Shock Wave Boundary Layer Interaction," *Shock Waves*, Vol. 19, 2009, pp. 163–169. doi:10.1007/s00193-009-0209-7

[25] Thomas, F., Putman, C., and Chu, H., "On the Mechanism of Unsteady Shock Oscillation in Shock/Wave Turbulent Boundary Layer Interaction," *Experiments in Fluids*, Vol. 18, Nos. 1–2, 1994, pp. 69–81. doi:10.1007/BF00209362

[26] Pirozzoli, S., and Grasso, F., "Direct Numerical Simulation of

Impinging Shock Wave/Turbulent Boundary Layer Interaction at $M = 2.25$," *Physics of Fluids*, Vol. 8, 2006, pp. 1–17.
[27] Garnier, E., and Sagaut, P., "Large Eddy Simulation of Shock/Boundary-Layer Interaction," *AIAA Journal*, Vol. 40, No. 10, 2002, pp. 1935–1944. doi:10.2514/2.1552
[28] Dupont, P., Debiève, J.-F., Dussauge, J. P., Ardissonne, J. P., and Haddad, C., "Unsteadiness in Shock Wave/Boundary Layer Interaction," Aérodynamique des Tuyères et Arrières-Corps Working Group, TR, ONERA, Sept. 18, 2003.
[29] Garnier, E., "Stimulated Detached Eddy Simulation of Three-Dimensional Shock/Boundary Layer Interaction," *Shock Waves*, Vol. 19, No. 6, 2009, pp. 479–486. doi:10.1007/s00193-009-0233-7
[30] Touber, E., and Sandham, N. D., "Low-Order Stochastic Modelling of Low-Frequency Motions in Reflected Shock-Wave/Boundary-Layer Interactions," *Journal of Fluid Mechanics*, Vol. 671, 2011, pp. 417–465. doi:10.1017/S0022112010005811
[31] Lin, J., and Howard, F., "Turbulent Flow Separation Control Through Passive Techniques," *AIAA Second Shear Flow Conference*, AIAA Paper 89-0976, 1989.
[32] Raghunathan, S., "Passive Control of Shock-Boundary Layer Interaction," *Progress in Aerospace Sciences*, Vol. 25, No. 3, 1988, pp. 271–296. doi:10.1016/0376-0421(88)90002-4
[33] Smith, A., and Babinsky, H., "Shock-Wave/Boundary-Layer Interaction Control Using Streamwise Slots in Transonic Flows," *Journal of Aircraft*, Vol. 41, No. 3, 2004, pp. 540–546. doi:10.2514/1.11479
[34] Lapsa, A. P., "Experimental Study of Passive Ramps for Control of Shock/Boundary Layer Interactions," Ph.D. Thesis, University of Michigan, 2009.
[35] Lee, S., Goettke, M. K., Loth, E., Tinapple, J., and Benek, J., "Microramps Upstream of an Oblique-Shock Boundary Layer Interaction," *AIAA Journal*, Vol. 48, No. 1, 2010, pp. 104–118. doi:10.2514/1.41776
[36] Deleuze, L., "Structure d'une Couche Limite Turbulente Soumise à une Onde de Choc Incidente," Ph.D. Thesis, Université Aix-Marseille II, Marseille, France, 1995.
[37] Laurent, H., "Turbulence d'une Interaction Onde de Choc/Couche Limite sur une Paroi Plane Adiabatique ou Chauffée," Ph.D. Thesis, Université Aix-Marseille II, Marseille, France, 1996.
[38] Germano, M., Piomelli, U., Moin, P., and Cabot, W. H., "A Dynamic Subgrid-Scale Eddy Viscosity Model," *Physics of Fluids A*, Vol. 3, 1991, p. 1760. doi:10.1063/1.857955
[39] Lilly, D. K., "A Proposed Modification of the Germano Subgrid-Scale Closure Method," *Physics of Fluids A*, Vol. 4, No. 3, 1992, p. 633. doi:10.1063/1.858280
[40] Moin, P., Squires, K., Cabot, W., and Lee, S., "A Dynamic Subgrid-Scale Model for Compressible Turbulence and Scalar Transport," *Physics of Fluids A*, Vol. 3, 1991, pp. 2746–2757. doi:10.1063/1.858164
[41] Mittal, R., and Moin, P., "Stability of Upwind-Based Finite Difference Schemes for Large-Eddy Simulation of Turbulent Flows," *AIAA Journal*, Vol. 35, 1997, pp. 1415–1417. doi:10.2514/2.253
[42] Garnier, E., Mossi, M., Sagaut, P., Comte, P., and Deville, M., "On the Use of Shock-Capturing Schemes for Large-Eddy Simulation," *Journal of Computational Physics* Vol. 153, 1999, pp. 273–311. doi:10.1006/jcph.1999.6268
[43] Adams, N. A., and Shariff, K., "A High-Resolution Hybrid Compact-ENO Scheme for Shock-Turbulence Interaction Problems," *Journal of Computational Physics*, Vol. 127, 1996, pp. 27–51. doi:10.1006/jcph.1996.0156
[44] Pirozzoli, S., "Conservative Hybrid Compact-WENO Schemes for Shock-Turbulence Interaction," *Journal of Computational Physics*, Vol. 178, 2002, pp. 81–117. doi:10.1006/jcph.2002.7021
[45] Ren, Y.-X., Liu, M., and Zhang, H., "A Characteristic-Wise Hybrid Compact-ENO Scheme for Solving Hyperbolic Conservation Laws," *Journal of Computational Physics*, Vol. 192, 2003, pp. 365–386. doi:10.1016/j.jcp.2003.07.006
[46] Hill, D. J., and Pullin, D. I., "Hybrid Tuned Center-Difference-WENO Method for Large Eddy Simulations in the Presence of Strong Shocks," *Journal of Computational Physics*, Vol. 194, No. 2, 2004, pp. 435–450. doi:10.1016/j.jcp.2003.07.032
[47] Pantano, C., Deiterding, R., Hill, D. J., and Pullin, D. I., "A Low Numerical Dissipation Patch-Based Adaptive Mesh Refinement Method for Large-Eddy Simulation of Compressible Flows," *Journal of Computational Physics* Vol. 221, 2007, pp. 63–87. doi:10.1016/j.jcp.2006.06.011
[48] Chao, J., Haselbacher, A., and Balachandar, S., "A Massively Parallel Multi-Block Hybrid Compact-WENO Scheme for Compressible Flows," *Journal of Computational Physics*, Vol. 228, 2009, pp. 7473–7491. doi:10.1016/j.jcp.2009.07.005
[49] Shu, C. W., and Osher, S., "Efficient Implementation of Essentially Non-Oscillatory Shock-Capturing Schemes," *Journal of Computational Physics*, Vol. 77, 1988, pp. 439–471. doi:10.1016/0021-9991(88)90177-5
[50] Touber, E., "Unsteadiness in Shock-Wave/Boundary-Layer Interactions," Ph.D. Thesis, University of Southampton, Southampton, United Kingdom, 2010.
[51] Pirozzoli, S., Grasso, F., and Gatski, T. B., Direct Numerical Simulation and Analysis of a Spatially Evolving Supersonic Turbulent Boundary Layer at $M = 2.25$," *Shock Waves*, Vol. 16, No. 3, 2004, pp. 530–545. doi:10.1063/1.1637604
[52] Guarini, S., Moser, R., Shariff, K., and Wray, A., "Direct Numerical Simulation of a Supersonic Turbulent Boundary Layer at Mach 2.5," *Journal of Fluid Mechanics*, Vol. 414, 2000, pp. 1–33. doi:10.1017/S0022112000008466
[53] Gaviglio, J., "Reynolds Analogies and Experimental Study of Heat Transfer in the Supersonic Boundary Layer," *International Journal of Heat and Mass Transfer*, Vol. 30, 1987, pp. 911–926. doi:10.1016/0017-9310(87)90010-X
[54] Pirozzoli, S., Larsson, J., Nichols, J. W., Bernardini, M., Morgan, B. E., and Lele, S. K., "Analysis of Unsteady Effects in Shock/Boundary Layer Interactions," *Proceedings of the 2010 Summer Program*, Center for Turbulence Research, Stanford University, CA, 2010.
[55] Pirozzoli, S., and Bernardini, M., "Direct Numerical Simulation Database for Impinging Shock Wave/Turbulent Boundary-Layer Interaction," *AIAA Journal*, Vol. 49, No. 6, 2011, pp. 1307–1312. doi:10.2514/1.J050901
[56] Morgan, B., Kawai, S., and Lele, S. K., "Large-Eddy Simulation of an Oblique Shock Impinging on a Turbulent Boundary Layer," AIAA Paper 2010-4467, 2010.
[57] Touber, E., and Sandham, N. D., "Comparison of Three Large-Eddy Simulations of Shock-Induced Turbulent Separation Bubbles," *Shock Waves*, Vol. 19, No. 6, 2009, pp. 469–478. doi:10.1007/s00193-009-0222-x
[58] Willmarth, W., and Yang, C. S., "Wall-Pressure Fluctuations Beneath Turbulent Boundary Layers on a Flat Plate and a Cylinder," *Journal of Fluid Mechanics*, Vol. 41, 2006, pp. 47–80. doi:10.1017/S0022112070000526

P. Tucker
Associate Editor